

# Chemical Science

Accepted Manuscript

This article can be cited before page numbers have been issued, to do this please use: L. Xu, Z. Zhang, H. Zhou, Z. Wen, Y. Liu, H. Dong and W. Xie, *Chem. Sci.*, 2026, DOI: 10.1039/D5SC08053C.



This is an Accepted Manuscript, which has been through the Royal Society of Chemistry peer review process and has been accepted for publication.

Accepted Manuscripts are published online shortly after acceptance, before technical editing, formatting and proof reading. Using this free service, authors can make their results available to the community, in citable form, before we publish the edited article. We will replace this Accepted Manuscript with the edited and formatted Advance Article as soon as it is available.

You can find more information about Accepted Manuscripts in the [Information for Authors](#).

Please note that technical editing may introduce minor changes to the text and/or graphics, which may alter content. The journal's standard [Terms & Conditions](#) and the [Ethical guidelines](#) still apply. In no event shall the Royal Society of Chemistry be held responsible for any errors or omissions in this Accepted Manuscript or any consequences arising from the use of any information it contains.

## ARTICLE

## Precise Graphitic Nitrogen-Incorporation by Electrochemical Oxidation

Leilei Xu<sup>[a]</sup>, Zhibo Zhang<sup>[a]</sup>, Hong Zhou<sup>[b]</sup>, Ziqi Wen<sup>[c]</sup>, Yuxuan Liu<sup>[a]</sup>, Heng Dong<sup>\*[a]</sup>, Wei Xie<sup>\*[b]</sup>Received 00th January 20xx,  
Accepted 00th January 20xx

DOI: 10.1039/x0xx00000x

Graphitic nitrogen (graphitic-N) plays a very important role in energy conversion and environmental protection. Although various synthesizing methods have been developed, complex devices and harsh conditions are often needed causing difficulty in flexible regulation. Electrochemical approaches are attracting increasing attention due to their mild reaction conditions, controllability, and environmental compatibility. However, precisely incorporating graphitic-N remains a significant challenge. This study designed a synthesis strategy that creating carbon single vacancies via electrochemical oxidation and then incorporating N radicals to construct graphitic-N. Graphite paper doped with exclusive graphitic-N was achieved by using ammonium ions as the nitrogen source. By integrating multiple operando electrochemical characterization techniques and density functional theory calculations, the crucial regulation parameters were clarified and the proposed doping mechanism was validated. Hydroxyl radicals generating from electrochemical water dissociation performed three functions including: evolving (i) carbon single vacancies and (ii) adjacent oxygen-containing functional groups, as well as (iii) activating ammonium ions into N-radicals. Ketone exhibited superior thermodynamic behavior than hydroxyl when assembling N radicals into carbon single vacancies. The findings offer both experimental and theoretical foundations for a deeper understanding of the structure-property relationships of graphitic-N and broaden the application prospects of graphitic-N-doped materials.

## Introduction

Graphitic-N denotes nitrogen atoms replacing sp<sup>2</sup>-hybridized carbon atoms in the hexagonal lattice of graphene. This is a typical in-plane nitrogen doping, where the radius of the nitrogen (N) atom (0.74 Å) is close to that of a carbon (C) atom (0.77 Å), thus preserving the coplanarity and conjugated structure of the carbon framework.<sup>1–3</sup> Owing to its higher electronegativity (3.04) relative to carbon (2.55), nitrogen doping—particularly in the form of graphitic-N—alters the local electronic environment within the carbon matrix. Graphitic-N, which acts as an electron-donating species, induces an upward shift of the Fermi level.<sup>4–6</sup> This electronic modulation enhances interfacial interactions governed by Lewis acid–base sites and  $\pi$ – $\pi$  stacking, thereby improving the material's reactivity in surface-related processes.<sup>7</sup> For instance, graphitic-N demonstrates a specific adsorption location to peroxide by forming a meta-stable intermediate with carbon plane.<sup>8</sup> It paves

the way for the development of non-radical advanced oxide process based on direct electron transfer, which possesses stronger selectivity to electron-rich emerging contaminants.<sup>9–11</sup> In addition, graphitic-N doped carbon cathode displays metal-like catalytic activity for the four-electron oxygen reduction reaction (ORR) and offers superior resistance to methanol crossover.<sup>12, 13</sup> It evidences that carbon materials are a promising alternative for non-metal cathodes in fuel cells.

A variety of physical-chemical methods for graphitic-N synthesis have been reported, including chemical vapor deposition,<sup>14, 15</sup> thermal methods,<sup>10, 11, 16</sup> plasma method,<sup>17</sup> etc. However, these approaches typically require harsh reaction conditions and complex devices, involving high temperatures, high vacuum, toxic or explosive reagents, and extended processing time. In contrast, electrochemical methods are receiving growing attention, relying on their outstanding advantages in mild reaction conditions, strong controllability and greater potential for industrial production. Common electrochemical techniques such as chronopotentiometry, voltammetry, and chronoamperometry have been adopted to dope nitrogen atoms into graphite-based materials under normal temperature and pressure. Multiple readily available nitrogen sources, including inorganic NH<sub>4</sub><sup>+</sup>/NO<sub>3</sub><sup>–</sup><sup>18–23</sup> and organic compounds (e.g., ionic liquids,<sup>24</sup> glycine,<sup>25</sup> melamine<sup>26</sup>), were employed in those studies.

Although nitrogen-doping has been successfully realized in electrochemical systems, mixed co-doping of pyridinic, pyrrolic,

<sup>a</sup> MOE Key Laboratory of Pollution Processes and Environmental Criteria, College of Environmental Science and Engineering, Nankai University, Tianjin 300350, China.

<sup>b</sup> State Key Laboratory of Advanced Chemical Power Sources, Key Laboratory of Advanced Energy Materials Chemistry (Ministry of Education), Tianjin Key Lab of Biosensing & Molecular Recognition, Haihe Laboratory of Sustainable Chemical Transformations, Renewable Energy Conversion and Storage Center, Frontiers Science Center for New Organic Matter, College of Chemistry, Nankai University, Tianjin 300071, China.

<sup>c</sup> College of Materials Science and Engineering, Nankai University, Tianjin 300350, China.



and graphitic nitrogen was generally obtained. Graphitic-N is a typical n-type doping which can effectively improve carrier density and conductivity of the carbon materials. So it is a favorable structure modification for the graphite electrode used in electrochemical energy-storage applications. However, pyridinic-N and pyrrolic-N act as p-type doping, which tends to induce carrier scattering and increase resistance, thereby hindering conductivity-oriented device performance. Therefore, the aim of this work is to incorporate graphitic-N into the carbon framework precisely. In addition, the current research progress regarding the synergistic interaction between electrolysis mode and nitrogen species was still unclear. In particular, real-time control over the site-specific evolution mechanisms involved in the graphitic-N formation remains a challenge, thereby limiting the tunability of the graphitic-N content.

Given the apparent structure of the graphitic-N, i.e., nitrogen atom substituting for one  $\text{sp}^2\text{-C}$  atom, we designed a controllable synthesis strategy consisting of vacancy-making and nitrogen-filling. Specifically, carbon single vacancies (SVs) are first created on a graphite topological plane via electrochemical oxidation. After that, N radicals are produced by electrochemically activating the nitrogen-containing

electrolyte to occupy these SVs. Inorganic ammonium cation is one of the typical nitrogen sources with the advantages of being harmless and shelf-stable, compared to organic amine cations and nitrate anions. In addition to our previous research on the electrochemical ammonia oxidation,<sup>27, 28</sup> in this work, the electrooxidation of  $(\text{NH}_4)_2\text{SO}_4$  was adopted to obtain N radicals. Crucial electrochemical parameters which enable modulate the concentrations of SVs and N radicals were systematically examined. Advanced operando characterization techniques—including surface-enhanced Raman spectroscopy (SERS), electron paramagnetic resonance (EPR), differential electrochemical mass spectrometry (DEMS), and density functional theory (DFT) calculations were comparatively utilized. The results confirmed the feasibility of our strategy, and a sample with 100% doping of relative graphitic-N was achieved. The doping mechanism and tuning approach were expounded in detail. This work provides a platform for systematically investigating the structure–property relationships between graphitic-N content and material performance, offering theoretical insights for optimizing catalysts, electrode materials, and sensors.

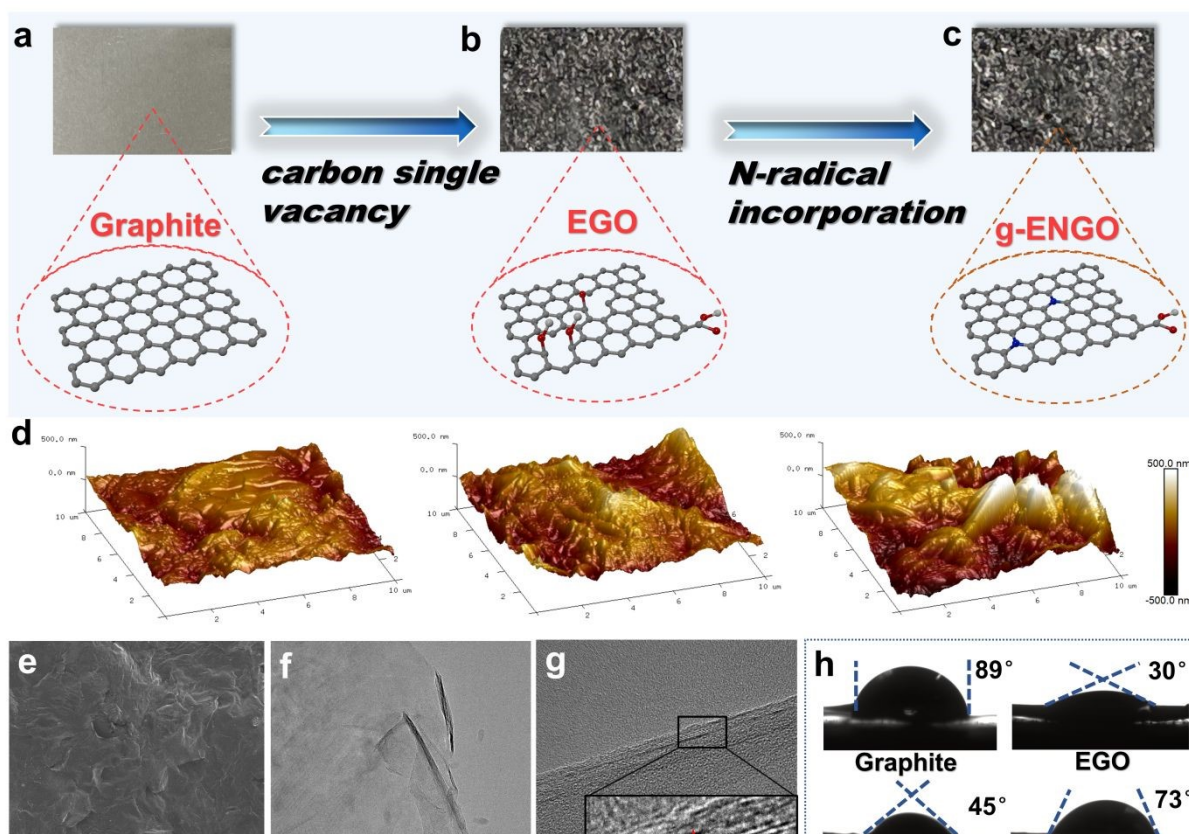


**Fig. 1** Catalyst preparation process: optical images and structural model of (a) graphite, (b) EGO, and (c) g-ENG. Atom representations are O (red), N (blue), and C (gray). (d) AFM morphological analysis of graphite, EGO, and g-ENG. (e) SEM images, and (f) (g) TEM images of g-ENG. (h) Contact angles of graphite, EGO, g-ENG, and g-ERNG.



Compared with traditional graphitic-N doping techniques, such as CVD, high-temperature annealing, and plasma treatment, our “consisting of vacancy-making and nitrogen-filling” electrochemical strategy exhibits notable advantages. This method operates under mild conditions (room temperature and pressure) and requires simple instrumentation and nontoxic reagents. By first generating carbon vacancies and subsequently introducing nitrogen radicals for selective filling, nitrogen atoms can directly substitute  $sp^2$ -C sites, enabling spatially localized and configuration-oriented doping. This effectively suppresses the co-formation of pyridinic-N and pyrrolic-N, allowing the generation of graphitic-N with a much higher phase purity than conventional approaches. In addition, doping parameters, including potential, current density, pulse design, and electrolyte composition can be tuned in real time, allowing programmable modulation of vacancy density and nitrogen-radical concentration. This offers precise control over both doping level and nitrogen configuration. Furthermore, this electrochemical environment is compatible with operando characterization (e.g., SERS, EPR, DEMS, DFT), enabling direct tracking of intermediate species and bonding evolution. Such capability strengthens mechanistic understanding and establishes a clearer structure–function correlation. Owing to its universality toward diverse carbon frameworks and scalable process conditions, this strategy shows strong potential for industrial application. Taken together, the method provides a precise, green, and scalable route for high-graphitic-N incorporation, offering advantages in both incorporation precision and mechanistic controllability.

## Results and Discussion

### Synthesis and Characterization

A strip of graphite paper (1.5 cm × 0.8 cm × 0.02 mm) was used as the work electrode (Fig. 1a), platinum wire and Ag/AgCl were respectively used as the counter electrode and reference electrode to construct a three-electrode cell. In the vacancy-making step, concentrated sulfuric acid (50 wt.%) was selected as the electrolyte and a constant potential of 1.8 V was applied. The oxidation period should be less than 30 min, or else the skeleton of graphite paper will be damaged into small fragments. Owing to the  $SO_4^{2-}$  intercalation as well as violent  $H_2O$  dissociation, lots of reactive oxidative radicals immediately grow up on the outer and inner surface of the graphite layers.<sup>29, 30</sup> They may contribute to the rapid formation of oxygen-containing functional groups (e.g., hydroxyl -OH, carbonyl -C=O, carboxyl -COOH) on the plane and edges and even the expected SV.<sup>31–33</sup> The sample obtained in this step is labeled as electrochemical graphene oxide (EGO) (Fig. 1b). In the nitrogen-filling step, the electrolyte was replaced by 1.25 M  $(NH_4)_2SO_4$  aqueous solution and an oxidation potential lower than 1.8 V was applied for 30 min. It is assumed that the nitrogen atom in the  $NH_4^+$  can be dehydrogenated and precisely filled into the SV as graphitic-N just like g-ENG0 plotted in Fig. 1c.

By comparing their optical photos, it can be seen that the shape of the graphite paper remained unchanged, suggesting its convenience when working as an electrode. However, they exhibit significant differences in the surface roughness. According to the detection of atomic force microscopy (AFM) (Fig. 1d), the graphite surface was relatively smooth with a roughness ( $R_a$ ) of  $\approx 0$  nm. After electrochemical oxidation, a few “stalactite”-like protrusions appeared on the surface of EGO, corresponding to an increased roughness ( $R_a$ ) of  $\approx 300$  nm. When the nitrogen atoms were assembled in the g-ENG0, these “stalactites” transformed into “ridge”-like distributions and the roughness ( $R_a$ ) increased to  $\approx 500$  nm. The surface morphology of the g-ENG0 was further observed using scanning electron microscopy (SEM) and transmission electron microscopy (TEM) (Fig. S2). From the SEM images with magnification of 100 times, obvious wrinkles can be observed, which probably result from the oxygen-containing functional groups generation and oxygen bubbles evolution (Fig. 1e). Under the TEM view with magnification of 63000 times (Fig. 1f), g-ENG0 looks like smooth gauze which is the typical morphology of a two-dimensional nanocarbon material. Because of the  $SO_4^{2-}$  intercalation, its lattice fringes spacing (0.46 nm) (Fig. 1g) is larger than the normal spacing of few-layer graphene (0.34 nm). A similar phenomenon can also be seen from the graphite paper with a thickness of 1 mm (Fig. S3).

As the surface characteristics of graphite were significantly altered after oxidation and N-doping, the hydrophilicity was correspondingly changed. According to the contact angle testing (Fig. 1h), graphite paper demonstrates the poorest hydrophilicity (contact angle:  $89^\circ$ ) because its non-polar surface characteristics weakly interact with polar water molecules. When a substantial number of oxygen-containing functional groups was introduced in the EGO, its surface polarity was significantly enhanced, exhibiting a great enhancement in hydrophilicity with a contact angle of  $30^\circ$ . Whereas, the hydrophobicity of the g-ENG0 was a little recovered (contact angle:  $45^\circ$ ), suggesting that the graphitic-N assembling may consume its adjacent oxygen-containing groups and partially restore the non-polar  $sp^2$  conjugated structure. The electrochemical reduction of g-ENG0 was performed to further remove some oxygen-containing functional groups (g-ERNG0). As expected, its hydrophobicity was continuously increased with a contact angle of  $73^\circ$ . These results support that the hydrophilicity of g-ENG0 can be flexibly adjusted in-situ by using the electrochemical method, which usually plays a key role in an aqueous chemical reaction.

### Precise regulation of graphite nitrogen

As the proposed hypothesis, forming SVs is the prerequisite for incorporating graphitic-N and a series of characterization techniques were adopted to verify their existence. EPR is a visual and quantitative method for determining the concentration of SVs in EGO (Fig. S4). It can be found from Fig.





2a that the characteristic peak pattern of the SV emerges at  $g$  factor of 2.003 and the content gradually increases as the oxidation time.<sup>34</sup> Especially in the first 10 min, SVs content rose from 0 to 1.493, indicating a relatively fast oxidation kinetics. Since the SV theoretically stems from carbon emission, operando DEMS in linear sweep voltammetry (LSV) mode for ten cycles was carried out to monitor and recognize the gaseous carbon molecules being released from the graphite planes. As shown in Fig. 2b, the signal with specific mass charge ratio ( $m/z$ ) of 28 (CO) and 44 (CO<sub>2</sub>) appeared repeatedly and stably in each cycle. In addition, the deconvoluted C1s and O1s spectra of XPS display three types of oxygen-containing functional groups including hydroxyl (–OH), carbonyl (–C=O) and carboxyl groups (–COOH) (Fig. S5b and 5c). Referring to the results described above, we predict that the formation of SV is accompanied by the detachment of –OH and –C=O, which is due to continuous electrochemical oxidation at 1.8 V. The C/O ratios and high-resolution O1s spectra obtained from XPS measurements (Fig. S5a) for EGO-5, EGO-10, EGO-20, and EGO-30 provide direct evidence for the prediction. As the electrochemical oxidation proceeds, the C/O ratios exhibit fluctuate up and down, not the linear-like declining trend appearing in the electrochemical exfoliating GO.<sup>30</sup>

Raman spectroscopy analysis (Fig. 2c) was further performed to characterize the carbon structure of the EGO. The overall  $I_D/I_G$  ratio shows a downward trend, indicating that as the oxidation time extended,  $sp^3$  carbon decreased and SV increased. Compared to the graphite, 2D band (2720  $cm^{-1}$ ) of the EGO undergoes a red shift, which also suggests the transformation of in-plane  $sp^2$  carbon to distorted  $sp^3$  carbon and the development of defects.<sup>35</sup> In addition to the typical D-band (1350  $cm^{-1}$ ) and G-band (1580  $cm^{-1}$ ) peaks, the characteristic peak for D' band was observed at 1611  $cm^{-1}$  for EGO. The intensity of the D' band, originating from a double resonance Raman feature induced by disorder and defects, has been reported to be a measure for distinguishing boundary-like defects ( $I_D/I_{D'} \sim 3.5$ ), vacancy-type defects ( $I_D/I_{D'} \sim 7$ ), and  $sp^3$ -type defects ( $I_D/I_{D'} \sim 13$ ) by comparing with the intensity of the D band. Herein, the ratio of  $I_D/I_{D'}$  increased as the oxidation duration from 3.958 (EGO-5) to 6.704 (EGO-30), indicating that the boundary-like defects gradually transformed into vacancy-type defects (Fig. 2e).<sup>36</sup> Meanwhile, 3D Raman mapping of the D peak from the EGO-30 within a square area of  $10 \mu m \times 10 \mu m$  displays uniform distribution of the vacancies on the graphite plane (Fig. 2d).

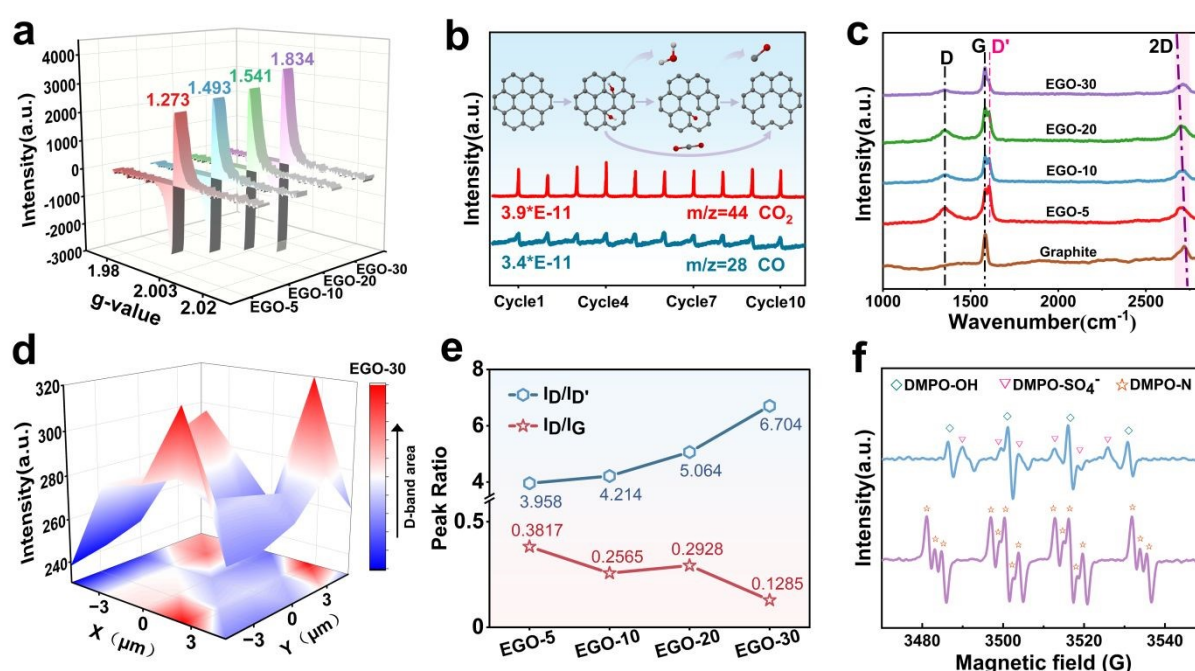


**Fig. 2** (a) EPR spectra of EGO. (b) Operando DEMS result of EGO. Atom representations are O (red), C (gray), and H (white). (c) Raman spectra. (d) D-band Raman mapping of EGO. (e)  $I_D/I_{D'}$  and  $I_D/I_G$  change curves. (f) Operando EPR spectra of DMPO-OH, DMPO-SO<sub>4</sub><sup>−</sup>, and DMPO-N during electrochemical processes.

Based on these results, it can be confirmed that SVs were successfully produced in the EGO and its concentration can be adjusted by controlling oxidation time.

Electrochemically activating  $\text{NH}_4^+$  to N radicals is the second step to form graphitic-N. The previous studies have speculated that hydroxyl radicals can attack ammonium ions to oxidation them into N radicals in an electrochemical system.<sup>37, 38</sup> In order to explore that by experiments, operando electrochemical EPR measurement was performed in LSV mode and 5,5-dimethyl-1-pyrroline-N-oxide (DMPO) was used as the trapping agent. As shown in Fig. 2f, EPR signals from DMPO-OH, DMPO- $\text{SO}_4^-$ , and DMPO-N spin adducts all appeared, indicating the formation of hydroxyl radicals, sulfate radicals, and N radicals ( $^*\text{NH}_2$  and/or  $^*\text{NH}$ ).<sup>39, 40</sup>

Precisely doping graphitic-N with controllable concentration is an anticipated advantage of the electrochemical method. Based on the prepared EGO at 1.8 V with different oxidation time (0~30 min), a series of g-ENG0 samples were prepared under a constant 1.6 V. From the deconvoluted N1s spectrum of the XPS (Fig. 3a, Fig. S7), the doped N states are composed of graphitic N (401.6 eV) and pyrrolic N (399.9 eV), without pyridine N (398.8 eV).<sup>16</sup> It is a significant difference compared to the chemical methods. By exploring the relationship between carbon vacancy content and the relative graphitic-N content (Fig. 3c), it was found that as carbon vacancy content increases, the relative graphitic-N content exhibits a trend of parabola. The highest 73% of the graphitic-N was obtained from g-ENG0-20. At this point, the absolute graphitic-N content also reaches 1.581% (Fig. S9). This is because an excessive oxidation duration

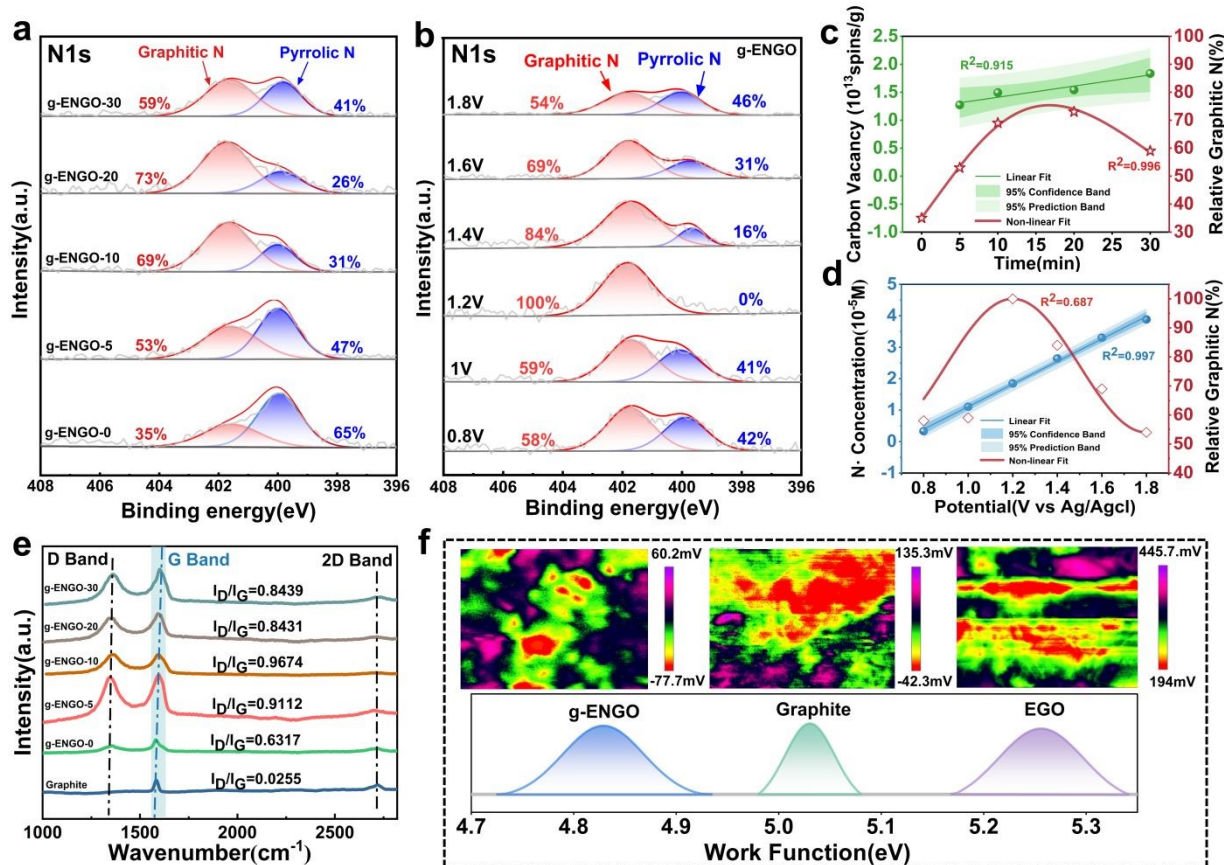


Fig. 3 (a) High-resolution XPS N1s of g-ENG0-x (x represents different oxidation times). (b) High-resolution XPS N1s of g-ENG0 (different doping potentials). (c) The relationship between carbon vacancies and relative graphitic N content as a function of oxidation time. (d) The relationship between nitrogen radicals and relative graphitic N content as a function of voltage. (e) Raman spectra. (f) Plots of work functions and potential maps of graphite, EGO, and g-ENG0 samples derived from KPFM results (inset).



will transform a carbon single vacancy into a double-vacancy or even hole defects, preventing nitrogen atoms from tridentate coordination.<sup>32</sup> Obviously, SVs are an essential condition for the formation of graphitic-N, which perfectly validates our hypothesis. Controlling the oxidation time of the EGO is one of the effective methods to adjust the graphitic-N content. The pioneers believed that pyrrolic-N occurs via the nucleophilic attack of N-containing species on the carbonyl functional groups.<sup>41</sup> Therefore, the lowest pyrrolic content of 26% in g-ENG0-20 can be attributed to the bottom level of its carboxyl functional groups (~0%) (Fig. S5). It can also be noted that even the graphite paper was doped by electrochemical oxidation without pre-oxidation (g-ENG0-0), graphitic-N still emerged, which confirms the effect of water dissociation on SVs generation. The negative results obtained from the methyl-added system also indicate the important effect of water dissociation (Fig. S11, Table S3).

As our prediction, anchoring the nitrogen atom into carbon, the N radical is another crucial process for constructing graphitic-N. When the distribution of the SV is determined, the N radical production is probably an adjustable parameter to control the concentration of graphitic-N in the g-ENG0. Since the oxidation potential has a significant influence on this process (Fig. S6), a series of doping potentials (0.8 V~1.8 V) for the g-ENG0 was examined with EGO-30 as the basic sample (Fig. 3b, Fig. S8). Similar to the influence of the oxidation time during EGO synthesis, the relative graphitic-N content also exhibited a parabola trend with the doping potential (Fig. 3d, Fig. S10). Specifically, 100% relative content of graphitic-N was obtained under 1.2 V, indicating that N radicals are another key factor in the formation of graphitic-N. A quantitative comparison with prior work including synthesis parameters, total nitrogen content, and nitrogen-species distribution are listed in Table S1. The advantage of our electrochemical method for the precise incorporation of graphitic-N can be clearly understood. According to the assumption from the contact angle test that oxygen-containing functional groups may be involved in graphitic-N formation, we conducted a nitrogen-doping experiment by pyrolyzing SV-contained graphite and melamine at 900°C (Fig. S12). Due to the lack of oxygen-containing functional groups on the graphite plane, not any nitrogen atom was doped in. It suggests that oxygen-contained functional groups are the third essential participants for graphitic-N assembling, especially the adjacent ones at the SV.

The incorporation of graphitic-N on the graphite plane was further validated via Raman spectroscopy (Fig. 3e) and Kelvin probe force microscopy (KPFM) using the series of g-ENG0 adjusted by oxidation time (Fig. 3f). Compared with the original graphite, the  $I_D/I_G$  ratio of the g-ENG0 increased significantly, confirming the gradual formation of defect structures due to nitrogen doping. In addition, the G band ( $1580\text{ cm}^{-1}$ ) of the g-ENG0 exhibits a blue shift, which is a typical demonstration of nitrogen doping in graphite.<sup>42</sup> Meanwhile, KPFM work function measurements testify the opposite regulatory effects of vacancy doping and graphitic-N doping on the Fermi level of graphene. Using work function ( $\Phi \approx 5.03\text{ eV}$ ) of the graphite as a reference, EGO gives a higher work function of  $\sim 5.26\text{ eV}$ ,

indicating a downward shift in the Fermi level. In contrast to that, g-ENG0-1.2 gives a lower work function of  $\sim 4.82\text{ eV}$ , indicating an upward shift in the Fermi level.<sup>43</sup>

### Synthesis mechanism

On the basis of the experimental results, the proposed mechanism regarding nitrogen transformation from ammonia ions to N radicals was further verified by SERS (Fig. 4a, Fig. S13). Detailed experimental procedures are provided in the Supporting Information. By performing LSV over a potential range of 0.8 V to 1.95 V (vs Ag/AgCl), we successfully detected the stretching vibration modes of  $^*\text{NH}_2$  ( $410\text{ cm}^{-1}$ ),  $^*\text{NH}$  ( $662\text{ cm}^{-1}$ ), and  $^*\text{NNH}$  ( $585\text{ cm}^{-1}$ ) which are key intermediates needed in the graphitic-N doping process.<sup>27, 28</sup> Additionally, the stretching vibration peak of the active oxygen radical ( $^*\text{O}$ ) was consistently observed at  $516\text{ cm}^{-1}$ . Within the voltage range of 0.8 V~1.7 V, the strong peak intensities of the  $^*\text{NH}_2$  and  $^*\text{O}$  peaks provide strong evidence that the primary N radicals are  $^*\text{NH}_2$  and they are achieved depending on the attack of the hydroxyl radicals on the ammonium ions. When the potential continuously rises to 1.9 V, the intensity of the  $^*\text{O}$  peak decreases and the  $^*\text{NH}_2$  peak disappears, indicating that excessive potential will cause vigorous hydrolysis, resulting in undesirable production of oxygen. Peaks corresponding to  $^*\text{NH}$  are also observed in the 0.8 V~1.7 V range and its intensity continuously increases with the potential. The similar trends between  $^*\text{NH}_2$  and  $^*\text{NH}$  indicate that the adsorbed  $^*\text{NH}_2$  undergoes a dehydrogenation reaction on the EGO surface to form  $^*\text{NH}$ . Additionally, the  $^*\text{NNH}$  peak becomes prominent in the range of 1.4 V and 1.7 V but nearly disappears when the potential continues to rise. It indicates that a significant portion of the adsorbed  $^*\text{NH}$  undergoes N–N coupling reactions to form  $\text{N}_2$ .<sup>28</sup>

DFT calculations were performed to clarify the reaction mechanism from EGO to g-ENG0 in the thermodynamic perspective (Fig. 4b and 4c). Given the experimental results above, we constructed two EGO models: a single carbon vacancy on a finite graphene flake with one carbonyl ( $-\text{C}=\text{O}$ ) group (EGO-1) or adjacent two hydroxyl ( $-\text{OH}$ ) groups (EGO-2) (Fig. S14). The three unsaturated carbon atoms surrounding the vacancy were labeled as  $\text{C}_1$ ,  $\text{C}_2$ , and  $\text{C}_3$  (Fig. 4b and Fig. S15). Route-a exhibited graphitic-N doping in EGO-1, localized amplification as a-INT1. The carbonyl group is bonded to  $\text{C}_1$ , and an external  $-\text{NH}_2$  group adsorbs onto the carbonyl site with a binding energy of  $3.03\text{ kcal}\cdot\text{mol}^{-1}$ . Subsequently, the nitrogen atom bonds with  $\text{C}_2$ , followed by the transfer of one hydrogen atom from  $-\text{NH}_2$  to the oxygen atom, forming an  $-\text{OH}$  group. The nitrogen then bonds with  $\text{C}_3$ , resulting in two new C–N bonds on the carbon surface. Finally, the nitrogen forms a bond with  $\text{C}_1$ , undergoing a second N–H dissociation (ab-INT2). The released hydrogen atom attacks the oxygen atom, forming an  $\text{H}_2\text{O}$  molecule and simultaneously completing the formation of graphitic-N (abc-INT2). Route-b and route-c were both calculated for graphitic-N doping in EGO-2 (bc-INT1). The two hydroxyl groups are bonded to  $\text{C}_1$  and  $\text{C}_3$ , and the  $-\text{NH}_2$  group adsorbs onto them with a binding energy of  $3.39\text{ kcal}\cdot\text{mol}^{-1}$ . The nitrogen atom sequentially bonds with  $\text{C}_2$  and  $\text{C}_1$ ,





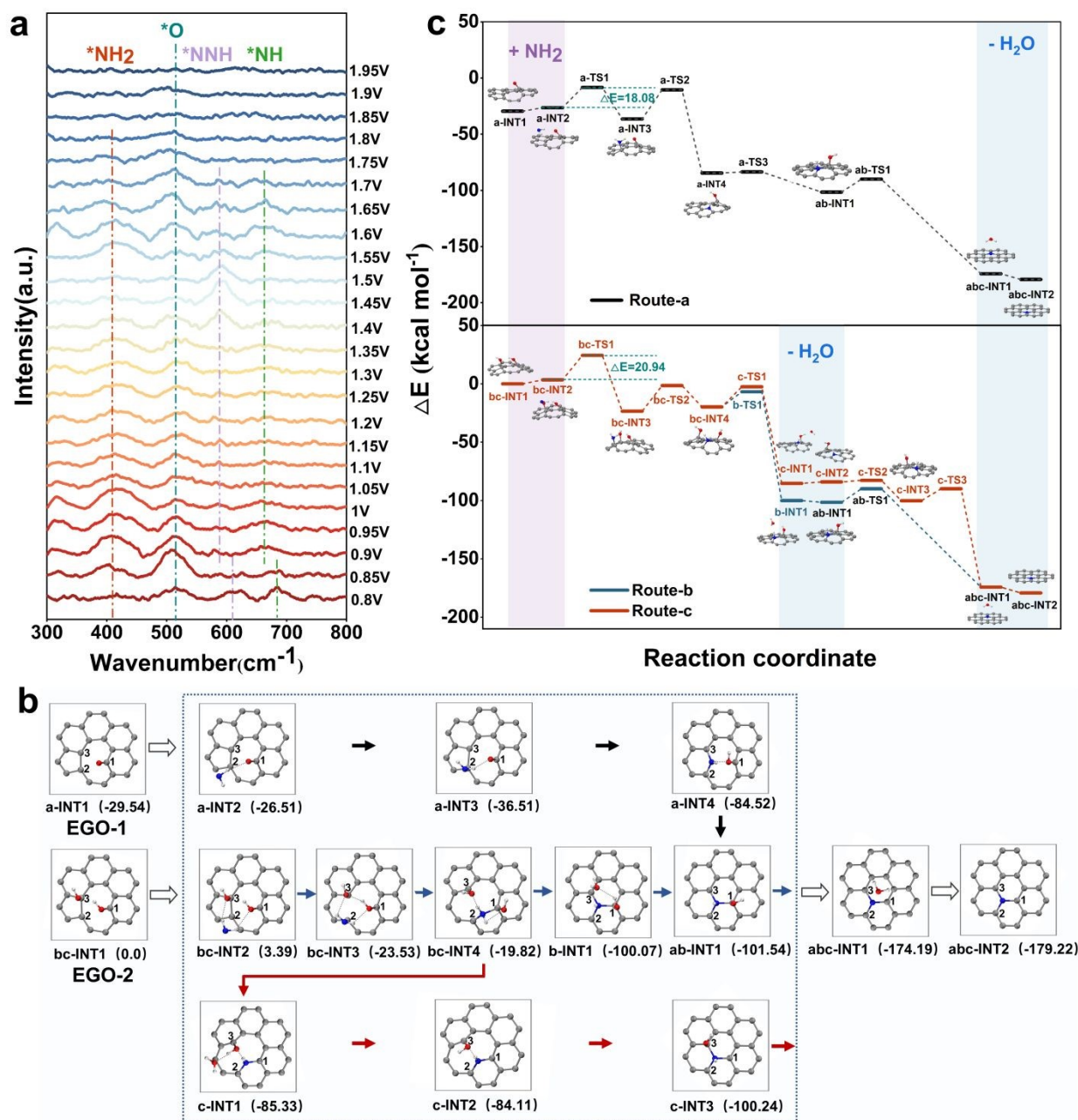


**Fig. 4** (a) SERS spectra of ammonia dehydrogenation in an aqueous solution of 1.25 M (NH<sub>4</sub>)<sub>2</sub>SO<sub>4</sub>. (b) Fragmental structures for the stationary points involved in route-a, route-b, and route-c. Atom representations are O (red), N (blue), C (gray), and H (white). Other carbon atoms are omitted for clarity. The distances are represented in units of angstroms. Relative energies (in parentheses) are given in kcal mol<sup>-1</sup>. (c) Reaction energy distribution of ammonia-mediated a-INT1 (route-a in black) and bc-INT1 (route-b in blue and route-c in red) doping reactions.

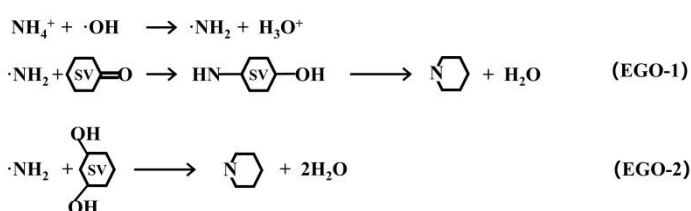




forming two C–N bonds and two –OH groups. The route bifurcates based on which oxygen atom the hydrogen in –NH<sub>2</sub> attacks first. In route-b, the nitrogen bonds with C<sub>3</sub>, and the hydrogen attacks the oxygen on C<sub>3</sub> to form an H<sub>2</sub>O molecule. A second N–H cleavage then occurs, with hydrogen attacking the oxygen on C<sub>1</sub>, generating a second H<sub>2</sub>O molecule and resulting in graphitic-N formation (abc-INT2). In route-c, the hydrogen atom first attacks the oxygen on C<sub>1</sub>, forming H<sub>2</sub>O, followed by nitrogen bonding with C<sub>3</sub>. A second N–H cleavage yields another H<sub>2</sub>O molecule through attack on the oxygen at C<sub>3</sub>, again resulting in graphitic-N.

As shown in Fig. 5c, in all three routes (a, b, and c), the attachment of the –NH<sub>2</sub> group to the carbon atom (a-TS1 and bc-TS1) is the rate-determining step, with activation energies of 18.08 kcal·mol<sup>–1</sup> for route a and 20.94 kcal·mol<sup>–1</sup> for routes b and c. These values suggest that graphitic-N doping is kinetically accessible in all three cases. The calculated reaction energies are –149.68 kcal·mol<sup>–1</sup> for route a and –179.22 kcal·mol<sup>–1</sup> for routes b and c, confirming that the graphitic-N deriving from the SV, –NH<sub>2</sub> and adjacent oxygen-containing functional groups is thermodynamically favorable under electrochemical conditions.

Based on the experimental research and DFT calculation mentioned above, schematic equations for elucidating the mechanism that how NH<sub>4</sub><sup>+</sup> ions are converted into graphitic nitrogen under our electrochemical conditions are provided as follows:



### g-ENG0 Applications

In our previous research, the experiments and DFT calculation clearly showed that peroxydisulfate (PDS) can preferentially adsorb on

graphitic-N (–2.46 eV on graphitic-N, –1.30 eV on pyridinic-N and –1.34 eV on N vacancy).<sup>32</sup> It means that electron transfer can occur from graphitic-N to the PDS without any external energy input. It can be attributed to the raised Fermi level of the carbon material by the graphitic-N doping (proved by KPFM here). Therefore, we performed open-circuit potential (OCP) measurement for detecting the electron transfer from graphitic-N to PDS as a reference to evaluate the performance of the g-ENG0 obtained from different doping potentials (Fig. 5a). To avoid the interference of the oxygen-containing functional groups, the g-ENG0 was reduced at –1V for 30 min (Fig. S16). The initial OCP of g-ERNG0 remained stable, and upon injection of 1 mM PDS at 300 s, the OCP of g-ERNG0 immediately increased by 0.2 V–0.5 V. Especially, the amplification of OCP was positively correlated with the relative content of graphitic-N. This result gives a reliable prediction that g-ERNG0 can be used as an electrochemical sensor for PDS.

OER performance was also examined as a demonstration of the graphitic-N doping. LSV tests (Fig. 5b) show that the initial overpotentials of g-ERNG0–1.6 V, 1.4 V, 1.2 V, 1 V, and 0.8 V are 1.39 V, 1.41 V, 1.45 V, 1.51 V, and 1.63 V, respectively, significantly lower than that of graphite (1.84 V relative to RHE). In particular, the increase of absolute graphitic-N content has an obvious role in negatively shifting the overpotential of OER. Good stability of the g-ERNG0 was demonstrated through consecutive cyclic voltammetry (CV) scans for 50 cycles, indicating its application potential in practice (Fig. S18).

Since the active oxide radicals derived from OER are crucial for N radicals generation during g-ENG0 synthesis, we designed a masking experiment by using the operando EPR measurement (Fig. 5c) to verify the active role of graphitic-N on OER, in which EGO-5, EGO-10, EGO-20, and EGO-30 were used as the working electrode, and graphitic-N doping was performed by oxidizing them for 10 min in 1.25 M (NH<sub>4</sub>)<sub>2</sub>SO<sub>4</sub>. At the same time, the scavenger DMPO is added to the scavenging system to capture N radicals that are not used for doping. Theoretically, the peak intensity of the N radicals should decrease resulting from the capture by SVs in the graphite. However, as the content of SVs gradually increased from EGO-5 to EGO-30 (Fig. 2a), the concentration of the captured N radicals also exhibited an ascending trend. The reason may lie in that the graphitic-N generated during doping reduces the energy barrier for hydrolysis to hydroxyl, thereby promoting the accelerated production of N radicals. This is consistent with our predicted conclusion.



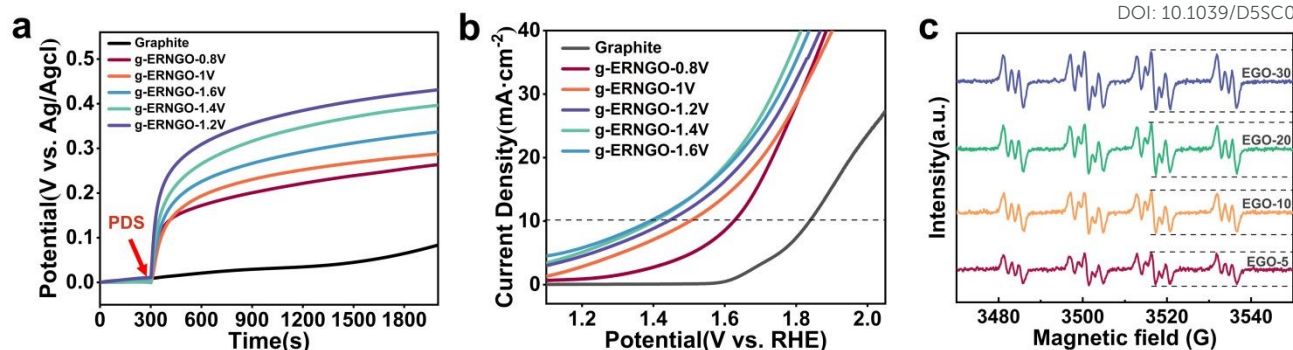


**Fig. 5** (a) Open-circuit potential curves with the addition of 1 mM PDS on g-ENGO-X (X represents the doping potential). (b) LSV curves of g-ENGO-X in 1 M KOH solution, showing the OER catalytic activity of the electrode. (c) Operando EPR spectra of DMPO-N during g-ENGO preparation.

## Conclusions

In this work, we proposed a controllable and easy-to-operate electrochemical method enabling selective synthesis of graphitic-N at ambient temperature and pressure. The sequence process containing vacancy engineering and N radical assembling allows precise regulation of graphitic-N content and 100% relative content of graphitic-N was achieved. By integrating advanced characterization and DFT calculation, we elucidated the formation mechanism of graphitic-N and identified the crucial parameters for precise regulation of graphitic-N. The SV, N radicals and adjacent oxygen-containing functional groups are the three essential participants for graphitic-N doping, which significantly depend on the electrochemical water dissociation to hydroxyl radicals. This study provides a flexible framework for the systematic preparation of nitrogen-doped carbon materials and paves the way for their application in electrochemical energy conversion (e.g., fuel cells, metal-air batteries), environmental remediation (e.g., advanced oxidation processes, pollutant adsorption), electrochemical sensing and so on—thereby contributing to the development of sustainable, green, and low-carbon technologies.

## Author contributions

Conceptualization: Leilei Xu, Heng Dong; investigation: Leilei Xu, Zhibo Zhang, Hong Zhou, Ziqi Wen; supervision: Heng Dong, Wei Xie; writing - original draft: Leilei Xu; writing - review & editing: Heng Dong, Wei Xie, Yuxuan Liu.

## Conflicts of interest

The authors declare no competing interests.

## Data availability

The data that support the findings of this study are available in the paper and SI. Supplementary information is available.

## Acknowledgements

The authors acknowledge the financial support from the National Natural Science Foundation of China (U24A20518 & 22574082), the Fundamental Research Funds for the Central Universities, Entrepreneurship Shenzhen Science and Technology Program (KCXFZ20211020172542001) and the 111 project (B25010).

## Notes and references

1. P. Błoński, J. Tuček, Z. Sofer, V. Mazánek, M. Petr, M. Pumera, M. Otyepka and R. Zbořil, Doping with Graphitic Nitrogen Triggers Ferromagnetism in Graphene, *Journal of the American Chemical Society*, 2017, **139**, 3171-3180.
2. Y.-F. Lu, S.-T. Lo, J.-C. Lin, W. Zhang, J.-Y. Lu, F.-H. Liu, C.-M. Tseng, Y.-H. Lee, C.-T. Liang and L.-J. Li, Nitrogen-Doped Graphene Sheets Grown by Chemical Vapor Deposition: Synthesis and Influence of Nitrogen Impurities on Carrier Transport, *ACS Nano*, 2013, **7**, 6522-6532.
3. K. Yokwana, B. Ntsendwana, E. N. Nxumalo and S. D. Mhlana, Recent advances in nitrogen-doped graphene oxide nanomaterials: Synthesis and applications in energy storage, sensor electrochemical applications and water treatment, *Journal of Materials Research*, 2023, **38**, 3239-3263.
4. M. Fan, Z.-Q. Feng, C. Zhu, X. Chen, C. Chen, J. Yang and D. Sun, Recent progress in 2D or 3D N-doped graphene synthesis and the characterizations, properties, and modulations of N species, *J. Mater. Sci.*, 2016, **51**, 10323-10349.



5. X. Ning, Y. Li, J. Ming, Q. Wang, H. Wang, Y. Cao, F. Peng, Y. Yang and H. Yu, Electronic synergism of pyridinic- and graphitic-nitrogen on N-doped carbons for the oxygen reduction reaction, *Chemical Science*, 2019, **10**, 1589-1596.
6. E. B. Yutomo, F. A. Noor and T. Winata, Effect of the number of nitrogen dopants on the electronic and magnetic properties of graphitic and pyridinic N-doped graphene – a density-functional study, *RSC Advances*, 2021, **11**, 18371-18380.
7. B. Başer, B. Yousaf, U. Yetis, Q. Abbas, E. E. Kwon, S. Wang, N. S. Bolan and J. Rinklebe, Formation of nitrogen functionalities in biochar materials and their role in the mitigation of hazardous emerging organic pollutants from wastewater, *Journal of Hazardous Materials*, 2021, **416**, 126131.
8. Y. Gao, G. Hu, J. Zhong, Z. Shi, Y. Zhu, D. S. Su, J. Wang, X. Bao and D. Ma, Nitrogen-Doped sp<sup>2</sup>-Hybridized Carbon as a Superior Catalyst for Selective Oxidation, *Angewandte Chemie International Edition*, 2013, **52**, 2109-2113.
9. Y.-X. Huang, L.-Q. Yu, K.-Y. Chen, H. Wang, S.-Y. Zhao, B.-C. Huang and R.-C. Jin, Biochar with self-doped N to activate peroxymonosulfate for bisphenol-A degradation via electron transfer mechanism: The active edge graphitic N site, *Chinese Chemical Letters*, 2024, **35**, 109437.
10. F. Li, L. Sun, H. Wang, H. Dong, F. Li, X. Wu and S. Zhan, Crucial role of nitrogen vacancies in carbon activated persulfate toward nonradical abatement of micropollutants from secondary effluent, *Applied Catalysis B: Environment and Energy*, 2025, **361**, 124584.
11. S. Zhu, X. Huang, F. Ma, L. Wang, X. Duan and S. Wang, Catalytic Removal of Aqueous Contaminants on N-Doped Graphitic Biochars: Inherent Roles of Adsorption and Nonradical Mechanisms, *Environmental Science & Technology*, 2018, **52**, 8649-8658.
12. T. Jeong, K. Kim, B. H. Kim, S. I. Choi, C. H. Choi, J. Kang and M. Kim, Ligand Engineering of Co-N<sub>4</sub> Single-Atom Catalysts for Highly - Active and Stable Acidic Oxygen Evolution, *Advanced Science*, 2025, **12**, e2502230.
13. G. Murdachaew and K. Laasonen, Oxygen Evolution Reaction on Nitrogen-Doped Defective Carbon Nanotubes and Graphene, *The Journal of Physical Chemistry C*, 2018, **122**, 25882-25892.
14. B. P. Jaisi, R. Zhu, G. Kalita and M. Umeno, Morphological changes of carbon thin films with nitrogen doping synthesized by microwave-excited surface wave plasma CVD, *Materials Chemistry and Physics*, 2023, **307**, 128183.
15. L. Lin, J. Y. Li, Q. H. Yuan, Q. C. Li, J. C. Zhang, L. Z. Sun, D. R. Rui, Z. L. Chen, K. C. Jia, M. Z. Wang, Y. F. Zhang, M. H. Rummeli, N. Kang, H. Q. Xu, F. Ding, H. L. Peng and Z. F. Liu, Nitrogen cluster doping for high-mobility/conductivity graphene films with millimeter-sized domains, *Sci. Adv.*, 2019, **5**, 9.
16. H. Kammoun, B. D. Osseonon and A. C. Tavares, Nitrogen-Doped Graphene Materials with High Electrical Conductivity Produced by Electrochemical Exfoliation of Graphite Foil, *Nanomaterials*, 2024, **14**, 123.
17. A. Bident, N. Caillault, F. Delange, C. Labrugere, G. Aubert, C. Aymonier, E. Durand, A. Demourgues, Y. Lu and J. F. Silvain, Nitrogen Radiofrequency Plasma Treatment of Graphene, *ChemistrySelect*, 2023, **8**, e202303661.
18. M. B. Arvas, M. Gencten and Y. Sahin, One-step synthesized N-doped graphene-based electrode materials for supercapacitor applications, *Ionics*, 2021, **27**, 2241-2256.
19. R. Bhaskaran and R. Chetty, One-Pot Room Temperature Synthesis of Nitrogen-Doped Graphene and Its Application as Catalyst Support for ORR in PEMFCs, *ACS Applied Energy Materials*, 2024, **7**, 390-402.
20. F. Lou, M. E. M. Buan, N. Muthuswamy, J. C. Walmsley, M. Rønning and D. Chen, One-step electrochemical synthesis of tunable nitrogen-doped graphene, *Journal of Materials Chemistry A*, 2016, **4**, 1233-1243.
21. X. Lu and C. Zhao, Controlled electrochemical intercalation, exfoliation and in situ nitrogen doping of graphite in nitrate-based protic ionic liquids, *Physical Chemistry Chemical Physics*, 2013, **15**, 20005-20009.
22. L. Magerusan, F. Pogacean and S. Pruneanu, Enhanced Acetaminophen Electrochemical Sensing Based on Nitrogen-Doped Graphene, *International Journal of Molecular Sciences*, 2022, **23**, 14866.
23. A. Shayesteh Zeraati, S. A. Mirkhani, F. Sharif, A. Akbari, E. P. L. Roberts and U. Sundararaj, Electrochemically Exfoliated Graphite Nanosheet Films for Electromagnetic Interference Shields, *ACS Applied Nano Materials*, 2021, **4**, 7221-7233.
24. X. Sun, N. Yang, H. Dong, H. Yu, H. Yu and L. Feng, In-situ electrochemical synthesis of heteroatoms-doped reduced graphene oxide toward nonradical degradation of tetracycline, *Chemical Engineering Journal*, 2023, **471**, 144834.
25. Y. Yang, W. Shi, R. Zhang, C. Luan, Q. Zeng, C. Wang, S. Li, Z. Huang, H. Liao and X. Ji, Electrochemical Exfoliation of Graphite into Nitrogen-doped Graphene in Glycine Solution and its Energy Storage Properties, *Electrochimica Acta*, 2016, **204**, 100-107.
26. F. Liu, F. Niu, T. Chen, J. Han, Z. Liu, W. Yang, Y. Xu and J. Liu, One-step electrochemical strategy for in-situ synthesis of S,N-codoped graphene as metal-free catalyst for oxygen reduction reaction, *Carbon*, 2018, **134**, 316-325.
27. M. Zhang, T. Wang, X. Du, Y. Mao, A. Zhu, A. Du, L. Tong and W. Xie, Observation of \*N<sub>2</sub>H<sub>3</sub> Intermediates by In Situ Electrochemical SERS: New Pathway of Ammonia Oxidation on High-Durability PtIr Catalysts, *Journal of the American Chemical Society*, 2025, **147**, 28331-28339.
28. X. Du, A. Du, D. Wang, Y. Mao, Z. Zhang and W. Xie, Surface-Enhanced Raman Spectroscopic Study of Key Intermediates in Electrochemical Ammonia Decomposition, *Journal of the American Chemical Society*, 2024, **147**, 8083-8087.
29. D. Chen, Z. Lin, M. M. Sartin, T.-X. Huang, J. Liu, Q. Zhang, L. Han, J.-F. Li, Z.-Q. Tian and D. Zhan, Photosynergetic Electrochemical Synthesis of Graphene Oxide, *Journal of the American Chemical Society*, 2020, **142**, 6516-6520.
30. S. Pei, Q. Wei, K. Huang, H.-M. Cheng and W. Ren, Green synthesis of graphene oxide by seconds timescale water electrolytic oxidation, *Nature Communications*, 2018, **9**, 145.
31. S. Fang, Y. Lin and Y. H. Hu, Recent Advances in Green, Safe, and Fast Production of Graphene Oxide via Electrochemical Approaches, *ACS Sustainable Chemistry & Engineering*, 2019, **7**, 12671-12681.
32. P. Feicht and S. Eigler, Defects in Graphene Oxide as Structural Motifs, *ChemNanoMat*, 2018, **4**, 244-252.





33. S. Yang, S. Brüller, Z.-S. Wu, Z. Liu, K. Parvez, R. Dong, F. Richard, P. Samorì, X. Feng and K. Müllen, Organic Radical-Assisted Electrochemical Exfoliation for the Scalable Production of High-Quality Graphene, *Journal of the American Chemical Society*, 2015, **137**, 13927-13932.
34. C. Jiang, Z. Chen, R. Yang, Z. Luogu, Q. Ren, H. Hu, K. Wang, S. Li, C. Deng, M. Li and L. Zheng, Carbon-Based Flexible Electrode for Efficient Electrochemical Generation of Reactive Chlorine Species in Tumor Therapy, *Advanced Healthcare Materials*, 2025, **14**, 2500369.
35. D. Belotckovtceva, R. P. Maciel, E. Berggren, R. Maddu, T. Sarkar, Y. O. Kvashnin, D. Thonig, A. Lindblad, O. Eriksson and M. V. Kamalakar, Insights and Implications of Intricate Surface Charge Transfer and  $sp^3$ -Defects in Graphene/Metal Oxide Interfaces, *ACS Applied Materials & Interfaces*, 2022, **14**, 36209-36216.
36. Y. Yamada, K. Murota, R. Fujita, J. Kim, A. Watanabe, M. Nakamura, S. Sato, K. Hata, P. Ercius, J. Ciston, C. Y. Song, K. Kim, W. Regan, W. Gannett and A. Zettl, Subnanometer Vacancy Defects Introduced on Graphene by Oxygen Gas, *Journal of the American Chemical Society*, 2014, **136**, 2232-2235.
37. J. Fan, L. Xie, X. Zhang, P. Zou, Y. Zheng, Y. Fan, H. Wang, X. Jiang and Y. Chang, Mechanically Induced Green Targeted Conversion of Ammonia Nitrogen to  $N_2$ : Based on Cavitation Effects and ROS Oxidation, *Environmental Science & Technology*, 2024, **58**, 21569-21577.
38. R. Halseid, J. S. Wainright, R. F. Savinell and R. Tunold, Oxidation of ammonium on platinum in acidic solutions, *J. Electrochem. Soc.*, 2007, **154**, B263-B270.
39. J. Dou, Y. Tang, Z. Lu, G. He, J. Xu and Y. He, Neglected but Efficient Electron Utilization Driven by Biochar-Coactivated Phenols and Peroxydisulfate: Polyphenol Accumulation Rather than Mineralization, *Environmental Science & Technology*, 2023, **57**, 5703-5713.
40. Q. Shi, W. Tang, K. Kong, X. Liu, Y. Wang and H. Duan, Electrocatalytic Upgrading of Plastic and Biomass-Derived Polyols to Formamide under Ambient Conditions, *Angewandte Chemie International Edition*, 2024, **63**, e202407580.
41. X. R. Wang, X. L. Li, L. Zhang, Y. Yoon, P. K. Weber, H. L. Wang, J. Guo and H. J. Dai, N-Doping of Graphene Through Electrothermal Reactions with Ammonia, *Science*, 2009, **324**, 768-771.
42. R. Arunpandian, M. Kumar, S. I. Lasalle B, P. Vijayakumar and J.-H. Chang, Hierarchical synthesis of multi-layer graphene-like and nitrogen-doped graphitized carbon from dead leaf biomass for high-performance energy storage and  $CO_2$  capture, *Journal of the Taiwan Institute of Chemical Engineers*, 2025, **172**, 106100.
43. P. Szroeder, A. Banaszak-Piechowska and I. Sahalianov, Tailoring Electrocatalytic Properties of  $sp^2$ -Bonded Carbon Nanoforms Through Doping, *Molecules*, 2025, **30**, 1265.

View Article Online  
DOI: 10.1039/D5SC08053C



**Data availability statements**

☒ The data supporting this article have been included as part of the Supplementary Information.

